SINGLE-SHOT QUANTITATIVE PHASE MICROSCOPY IN A COMMON-PATH CONFIGURATION

by

Brandon Norton

A thesis submitted to the faculty of
The University of North Carolina at Charlotte
in partial fulfillment of the requirements
for the degree of Master of Science in
Applied Physics

Charlotte

2023

Approved by:

_____
Dr. Rosario Porras-Aguilar

_____
Dr. Vasily Astratov

_____
Dr. Juan Vivero-Escoto

ABSTRACT

BRANDON NORTON. Single-Shot Quantitative Phase Microscopy in a Common-Path Configuration
(Under the direction of DR. ROSARIO PORRAS-AGUILAR)

Quantitative Phase Microscopy (QPM) is a technique frequently used in microscopy to gather information about transparent objects that provide a phase shift relative to their background. We propose a technique that employs a liquid crystal in a common-path configuration to provide quasi-real-time 3D information in a single shot. This technique involves using circularly polarized light and a polarized camera to produce 4 images corresponding to 4 different angles of linear polarization. These images can be combined to produce a phase map that contains 3D information about the object. This technique has the benefits of being robust to vibration, space-efficient, and relatively inexpensive.

ACKNOWLEDGMENTS

The work done in thesis would not have been possible without the financial support of the National Science Foundation (Award Number: 2047592), Research Corporation for Science Advancement, and the University of North Carolina at Charlotte Department of Physics and Optical Sciences.

I am especially grateful for the guidance, support, and knowledge my mentor, Dr. Rosario Porras, has given me. She gave me the opportunity and the help necessary to do science that I am proud of. I am thankful for each of the members on my advisory committee for their time and questions. In particular I want to thank Dr. Juan Vivero for providing the biological samples that were used in this thesis. I appreciate the help of all those I have had the pleasure of working with on this work and other projects. I would like to thank Mr. Bryce Evans, who tragically passed during my thesis work, for his friendship as well as his contribution to the experiments. He was a hardworking and warm person that will continue to be a source of inspiration for me. Most importantly, I want to thank my family for providing me with incredible opportunities and for their love and support in my pursuits.

TABLE OF CONTENTS

LIST OF FIGURES

LIST OF ABBREVIATIONS

AO	amplitude object
LC	liquid crystal
L	lens
MO	microscope objective
OI	object of interest
QPM	quantitative phase microscopy
QWP	quarter wave plate
PCM	phase contrast microscopy
PO	phase object

CHAPTER 1: INTRODUCTION

Biological specimens are nearly transparent objects that are difficult to image because they provide no amplitude modulation to the light and therefore are challenging to see in a conventional microscope. This problem is particularly pervasive in fields of biology, where it is necessary to image transparent objects such as cells. Figure 1 shows how light is affected by an amplitude object (AO) and a phase object (PO). The AO in Figure 1 ii) modulates only the amplitude of the light and not the phase. Therefore, light exiting the AO will be in phase with light that is unaffected, as shown in Figure 1 i). However, the light incident on the PO, shown in Figure 1 iii), will be phase modulated and out of phase with unaffected light. Figure 1 b) shows how a cell acts as a PO and modulates the phase of incident light depending on the local thickness of the cell.

Many techniques have been developed to image POs, including staining to turn the biosamples into amplitude objects, but staining has drawbacks. Staining involves using chemical components which is invasive, can take a long time to prepare, and can cause damage to the sample. Non-invasive techniques come with their own hurdles as well. Non-invasive optical imaging techniques must be used cautiously, as high illumination can cause damage to biological samples [1].

In the 1930s, Frits Zernike developed Phase Contrast Microscopy (PCM), in which the image contrast (the contrast between diffracted and undiffracted light) is enhanced due to shifting their relative phase by a quarter of a wavelength, as shown in Figure 2. Following phase shifting, measuring the relative power in the interferogram yields information regarding the shape of the object. Although PCM serves as a significant advance in contrast imaging by revealing details of transparent specimens without using any dye, the resulting phase-contrast image is an intensity distribution, i.e., the transparent object becomes visible. Although this technique is considered

non-invasive and label-free because it does not require the sample to be stained, the phase information cannot be decoupled and retrieved quantitatively from the intensity data [2].

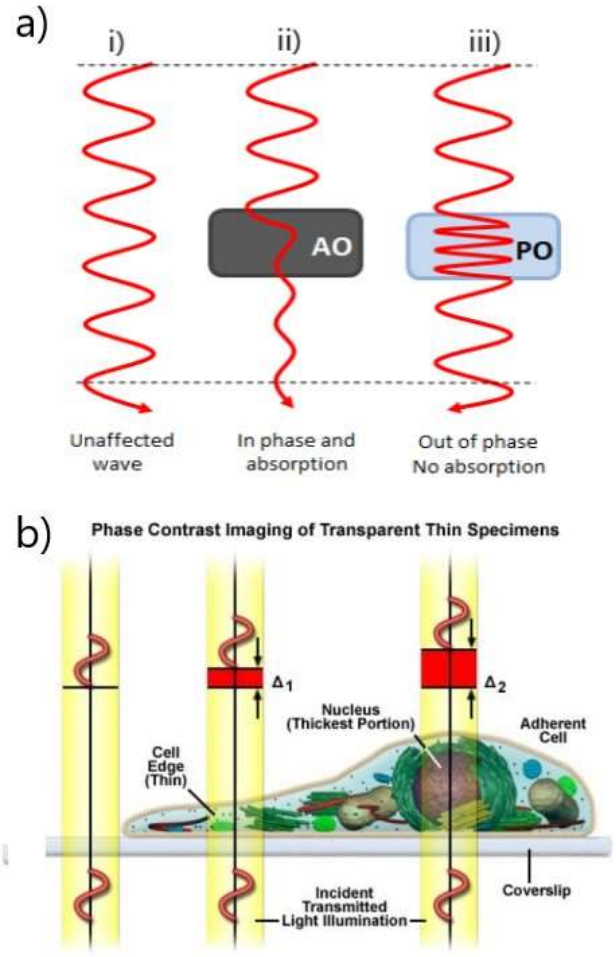

Figure 1
a) Optical waves propagating through i) no object so that neither amplitude nor phase are affected, ii) an AO that diminishes the amplitude but does not alter the phase, and iii) a PO that modulates the phase but does not change the amplitude. B) Optical waves propagating through a cell that acts as a quasi PO. Each wave experiences a different phase shift depending on the local thickness of the cell.

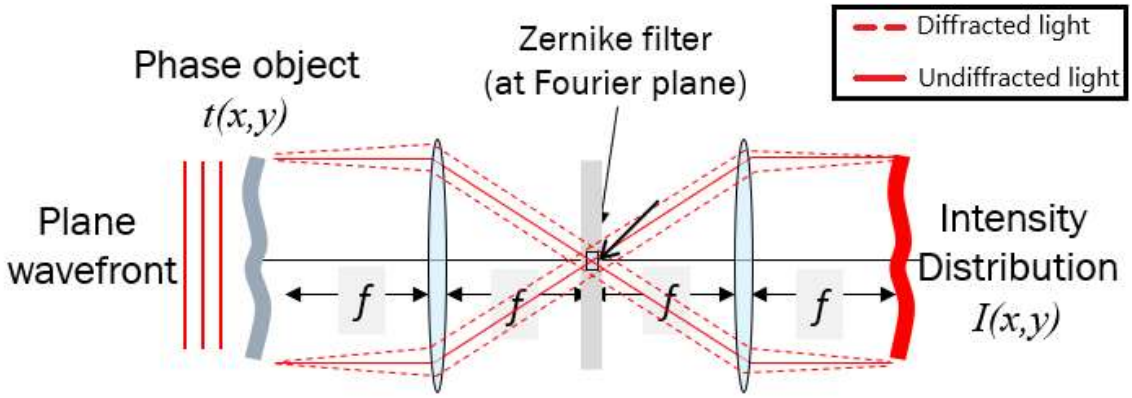

Figure 2
The CPC that Frits Zernike used to create PCM. A plane wave is incident on some phase object and, at the Fourier plane, a Zernike filter modulates the phase of the undiffracted light. After propagation from the Fourier plane, the undiffracted light interfers with the diffracted light to create phase contrast.

Other methods take advantage of interferometry and the optical phase delay caused by a transparent sample to create contrast in the amplitude. These methods include the use of optical elements that can spatially modulate light, such as SLMs [3], piezoelectric transducers [4], and nonlinear optical materials like liquid crystals [5]. These optical elements can be used in a Zernike configuration to produce an amplitude image of a PO [6]. Zernike configurations can be further improved to yield quantitative phase information.

Among all novel optical imaging techniques, quantitative phase microscopy (QPM) is one that has been widely explored by many researchers [1]–[4] and is commonly used in microscopy for imaging biological samples [10]. In contrast to PCM, QPM is capable of retrieving phase quantitatively, i.e., obtaining a surface map of the object of interest. This is the reason why QPM has shown various interesting biological applications and has become increasingly prevalent over the years. In QPM, the optical path-length map of a specimen is made, and the retrieved optical phase delay can be related to the physical and chemical properties of samples quantitatively [11].

Moreover, this QPM approach inherits the PCM benefits because staining is not needed. Thus, QPM is a non-invasive and label-free imaging approach [11].

The technique we propose to work on involves using an azobenzene liquid crystal, a circularly polarized beam, and a polarized camera for QPM in a common path configuration. The liquid crystal is a nonlinear optical material that can be used to modulate the phase of the zero-order light in the Fourier plane. The particular liquid crystal used in this thesis has strong nonlinear optical properties ($n_2 = 0.2\ \frac{\mathrm{cm}^2}{\mathrm{mW}}$) [12]. A strong nonlinear response is necessary because it allows the modulation of the zero-order light using low power, which prevents damage to biosamples. Additionally, the ability to use this apparatus with low-power illumination allows biosamples to be observed for long periods of time, which is necessary when studying biological processes that take days or weeks [13].

The polarized camera provides images at four different angles of polarization which, in combination with circularly polarized illumination, provides four phase-shifted images that can be used to calculate quantitative phase information [14]. This method is non-invasive, time-efficient, relatively inexpensive, resistant to environmental noise, and can provide pseudo real-time phase information of transparent objects.

Significance

There are several commercially available QPM devices on the market. Some of these devices are based on holographic measurements, which use holography to reconstruct the phase information of the light wave passing through the sample. However, as shown in the table below, the drawbacks of these technologies include i) the use of expensive optical elements, which

increases their cost, ii) the need for acquiring multiple images, resulting in a relatively slow system; and/or iii) the low-accuracy of the nanoscopic measurements (hundreds of nanometers).

Table 1

QPM Technology	Accuracy	Price
[15] **Phasefocus Livecyte**	40 nm	$150,000 to $200,000
[16] **Tomocube HT-2**	120 nm	$180,000 to $200,000
[17] **Lyncee Tec R1000**	100 nm	$70,000 to $100,000
[18] **Holomic Holographic**	500 nm	$20,000 to $30,000
[19] **PHI Holomonitor**	140 nm	€45,000 to €150,000 (Euro currency)
[20] **Phasics QPI**	Up to 5 nm	€70,000 to €150,000 (Euro currency)

This thesis aims to provide the proof-of-principle of QPM technology using inexpensive liquid crystal materials without sacrificing the accuracy of the measurements and low-intensity requirements for non-invasive bioimaging. An essential aspect of this work is to probe label-free quantitative microscopy in a single shot to enable dynamic 3D measurements and monitor biological processes in quasi-real time. Our ultimate goal is to develop a microscopy attachment with a compact, sturdy, and low-cost design that provides high accuracy in cell morphology estimation and easy integration with conventional microscopes.

CHAPTER 2: LITERATURE REVIEW

2.1 Phase Contrast Microscopy

One standard solution to the problem of imaging phase objects involves staining the biological samples so that structures in a sample are more visible in the microscope. However, this is not the preferred solution as staining is an invasive and often damaging technique. The chemicals that are used to stain the samples can alter and damage the structure of biological samples. Staining can also require time-consuming preparation processes. In addition, once the stain has been applied to a sample, the duration that the stain will be effective can be short, often on the order of minutes. In 1932 Frits Zernike discovered PCM, for which he later, in 1953, received the Nobel Prize in Physics. This technique involves exploiting the change in refractive index in a transparent object to obtain images that have more contrast in the object compared to brightfield microscopy. In contrast to staining, PCM is a time-efficient, non-invasive technique that does not damage biological samples.

For Zernike phase contrast, only small phase perturbations are considered, so the spatial phase distribution of a wave incident on a PO can be approximated using a first-order Taylor series approximation as follows,

$$U(x,y) = e^{i\phi(x,y)} \approx 1 + i\phi(x,y), \tag{1}$$

where $U(x,y)$ is the field and $\phi(x,y)$ is the spatial phase distribution [21]. Zernike realized that if a quarter-wave phase modulation is applied to the undiffracted light at the Fourier plane,

$$\hat{U}(k_x, k_y) \approx e^{i\frac{\pi}{2}}\delta(k_x, k_y) + i\hat{\phi}(k_x, k_y), \tag{2}$$

the resulting intensity distribution would be approximately linearly dependent on the phase distribution as shown in the following expression [21],

$$I(x,y) \approx \left|e^{i\frac{\pi}{2}} + i\phi(x,y)\right|^2 \approx 1 + 2\phi(x,y). \tag{3}$$

However, this is only an approximation for small phase objects and there are more all-encompassing models that consider higher order terms in the spatial phase distribution.

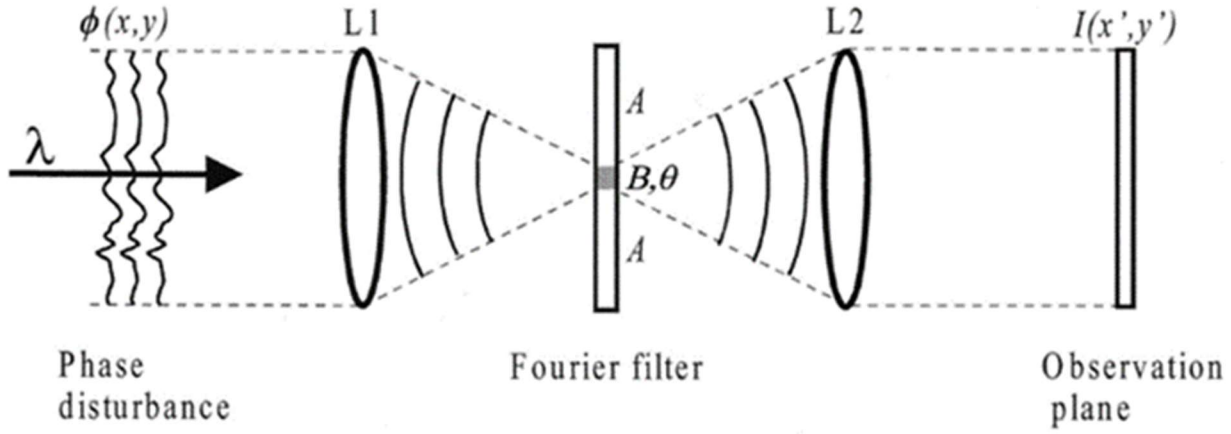

Figure 3
The setup for a point diffraction interferometer in a common path configuration. The phase disturbance is modulated by a Zernike phase filter at the Fourier plane to create an interference pattern at the observation plane. Reprinted from [21].

To implement PCM, an optical element is placed at the Fourier plane to modify the zero-order spatial frequency content. In other words, the undiffracted light is phase shifted, which then causes it to destructively interfere with the diffracted light at the image plane, creating a phase-contrast image. Implementations of PCM using active optical components such as spatial light

modulators (SLM) [3], piezoelectric transducers [4], and nonlinear optical materials like liquid crystals [22] have been demonstrated.

Many common interferometry techniques like shearing interferometry, holography, and phase estimation have problems with complexity both in the physical and computational implementation [23]. PCM systems are typically implemented in what is called a common path configuration (CPC). The common path approach has many benefits over other common interferometry techniques. One benefit of CPCs is their robustness against vibration, temperature changes, and other environmental disturbances. Since the reference beam and object beam share the same path, the path length difference for the reference beam will also be present in the object beam. Therefore, those changes will not affect the interference pattern as much. Another important benefit of CPCs is their simplicity. CPCs are more cost-effective, require fewer parts, typically require less space, and are more straightforward to implement. This makes CPCs apt for applications where stability and simplicity are important.

In this thesis, we will use a system similar to the point diffraction interferometer in a CPC, shown in Figure 3. The technique that we propose is based on liquid crystal materials that modulate the beam in a CPC and allow phase visualization.

2.2 Azobenzene Liquid Crystal Materials

Liquid crystal materials have an intermediate phase(s), mesophases, between their crystalline phase and isotropic liquid phase [24]. Liquid crystals in these mesophases exhibit properties of both a liquid and a crystal. These materials can be classified into the following three categories: lyotropic, polymeric, and thermotropic. [25]. In thermotropic liquid crystals, the

mesophase is induced via a temperature change. When the temperature of a thermotropic liquid crystal is raised above its melting temperature (T_M) and kept below its clearing temperature (T_C), it is in the liquid crystalline phase as shown in Figure 4.

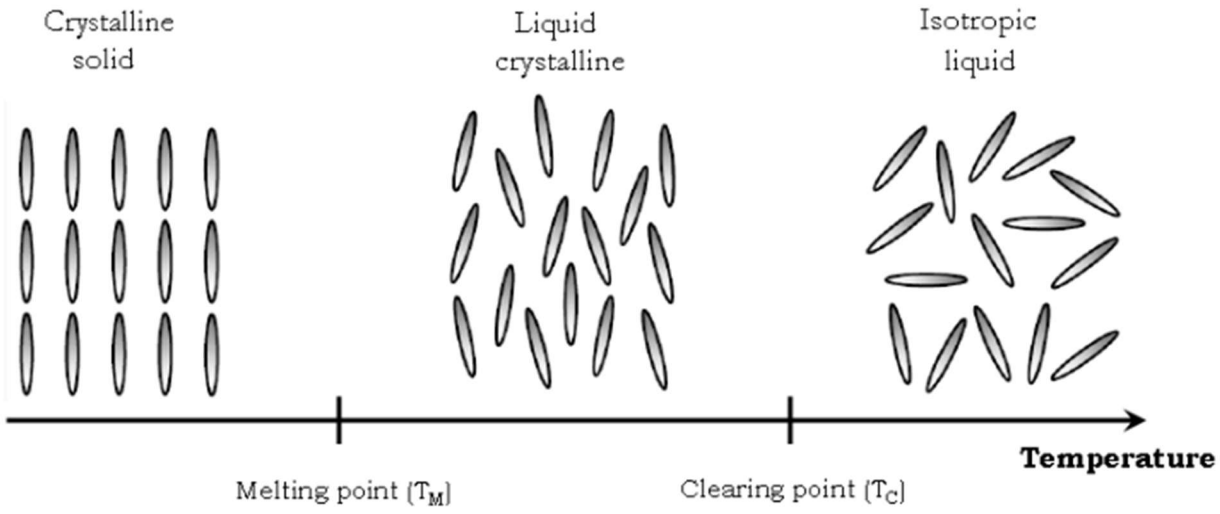

Figure 4
The crystalline solid phase, shown below T_M, has both positional order and orientational order. The liquid crystalline phase is reached once the temperature of the liquid crystal is raised above T_M. This phase has orientational order but not positional order. This allows it to flow like a liquid. The isotropic liquid phase is reached when the temperature is above T_C. The isotropic liquid has neither orientation nor positional order. Reprinted from [24].

Thermotropic liquid crystals are further classified into nematic, cholesteric, and smectic liquid crystals [24]. In nematic liquid crystals, the molecules have orientational order throughout the material but no positional order which allows them to flow like a liquid. The molecules also tend to be oriented in the same direction throughout the material. Therefore, nematic phases are typically said to be uniaxial. Cholesteric liquid crystals are similar to nematic phases in that they have no positional order and have some orientational order. Smectic phases differ from both

nematic and cholesteric liquid crystals in that they have some positional order. This work will focus on thermotropic, nematic liquid crystals.

One important property that will be leveraged in this research is the photoisomerization that occurs in azobenzene molecules. Photoisomerization occurs when light is incident on a material and induces a photoexcited state [26]. When light is incident on the azobenzene molecules, it can cause the trans isomers to switch to cis isomers [24]. However, the cis isomer is unstable and will return to the trans isomer after some period of time. The amount of photoisomerization is determined by the lifetime of the photoexcited state (the cis isomer in this case) in the molecules, and the response time of the molecules to the stimulus. The response time is a function of the quantum efficiency and absorption constants. The azobenzene molecules have a long photoexcited state and quick response time, which makes them ideal for photoisomerization [26].

The photoisomerization that occurs in these molecules can also be used to drastically intensify the nonlinear effects of liquid crystals [24]. Azobenzene dye can be added in small amounts to liquid crystals (azobenzene-dye doped liquid crystals) to induce a stronger reorientation of the dipoles in the liquid crystal molecules during photoisomerization of the dye [24], [27]. The torque on the liquid crystal molecules is significantly increased by anchoring cis isomers on the boundaries of the cell through dipole-dipole interactions [28], [29].

In this thesis, we use an azobenzene liquid crystal, which consists of a synthesized molecule that contains an azobenzene and a liquid crystal component [30]. This material exhibits a large optical nonlinearity and optical anisotropy, which makes this material a potential candidate for implementing quantitative phase microscopy. The intensity required to illuminate the object is reduced two orders of magnitude compared to QPM using azo-dye-doped liquid crystals [13]. In

addition, the optical anisotropy of azobenzene liquid crystals (the difference between the principal values of the refractive indices of the LC) is 0.20 at 633 nm wavelength.

2.3 Quantitative Phase Microscopy using Azobenzene Liquid Crystals

The photoisomerization and nonlinear optical effects of azobenzene liquid crystal materials can be exploited to create a self-modulating phase filter at the Fourier plane. This technique is shown in Figure 5. A common path configuration is used; however, at the Fourier plane, an azobenzene liquid crystal cell is used as the phase filter. This is an effective phase filter because only the undiffracted light at the Fourier plane will be of high enough intensity to cause photoisomerization in the liquid crystal, thereby acting as a self-modulating phase filter.

Typically, imaging systems will measure only amplitude information. However, quantitative phase imaging (QPM) is a technique used to gather phase information as well as amplitude information about a transparent object. This technique can be used to determine the 3D information of a transparent sample by using optical phase delay information [31]. QPM is a useful tool for the study of biological samples because it is both non-invasive and label-free [32] This is highly desirable in biological applications as it will not damage biological samples.

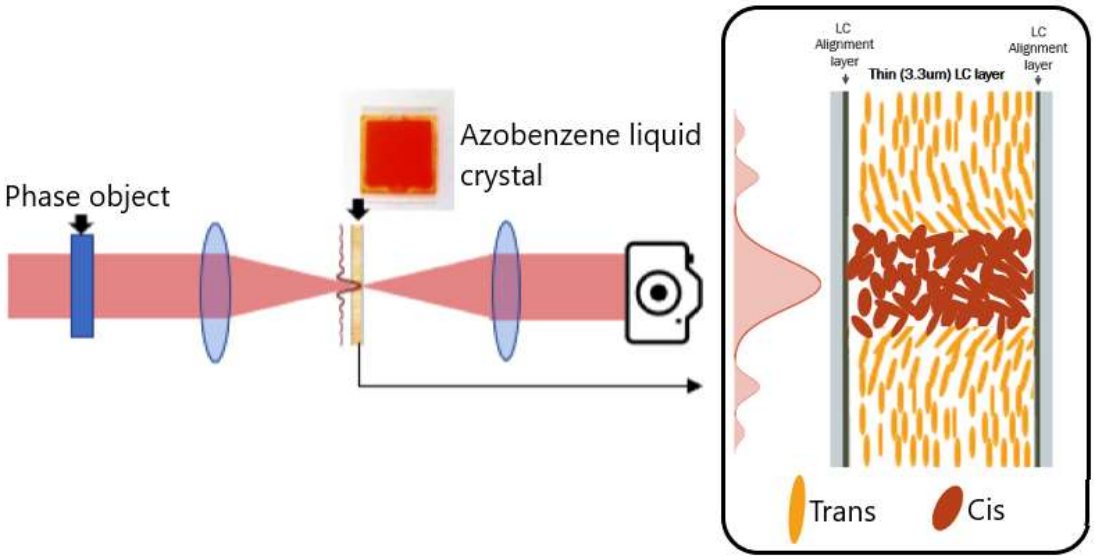

Figure 5
Same common path configuration shown in Figure 3, but implemented using a liquid crystal cell as the Fourier filter. The undiffracted light will be the greatest in intensity and will change the refractive index of the liquid crystal via photoisomerization. Reprinted from [22].

One technique that can be used to obtain quantitative phase information is the four-step technique [14]. This technique involves using phase shifting to obtain four intensity measurements with a quarter-wave shift between them. This can be written as,

$$I_{1(\mathrm{x,y})} = I_0(x,y)\{1+\gamma\cos(\phi(x,y))\}, \tag{4}$$

$$I_{2(\mathrm{x,y})} = I_0(x,y)\left\{1+\gamma\cos\left(\phi(x,y)+\frac{\pi}{2}\right)\right\}, \tag{5}$$

$$I_{3(\mathrm{x,y})} = I_0(x,y)\{1+\gamma\cos(\phi(x,y)+\pi)\}, \tag{6}$$

$$I_{4(\mathrm{x,y})} = I_0(x,y)\left\{1+\gamma\cos\left(\phi(x,y)+\frac{3\pi}{2}\right)\right\}, \tag{7}$$

where I_0 is the DC intensity, γ is the modulation of the interference fringes, and ϕ is the phase of the wavefront. Using these four measurements, the phase at each point in the image can be calculated using the following equation,

$$\phi(x,y) = \tan^{-1}\left(\frac{I_4 - I_2}{I_1 - I_3}\right). \tag{8}$$

CHAPTER 3: METHODS

The experimental apparatus, shown in Figure 6, consists of a 640 nm, 10 mW Coherent StingRay Laser Diode Module, a quarter-wave plate (QWP), a microscope objective (MO), two positive lenses, an azobenzene liquid crystal (LC), and the FLIR BFS-U3-51S5P-C camera. The LC material is azobenzene LC, 4955 by Beam Co [12]. The nonlinear coefficient of the LC material for 532 nm light, with parallel polarization relative to the molecular orientation and a cell gap of 10 mm, is $n_2 = 2.1 \times 10^{-1}$ cm^2/W. The FLIR camera has a resolution of 2448×2048 with a pixel pitch of 3.45 µm×3.45 µm. Images consist of groups of 2×2 pixels called superpixels. Each pixel in the superpixel takes a measurement for a particular polarization angle. The 2448×2048 size image generated by the camera can be separated into four individually polarized images captured simultaneously.

The LC is a nonlinear optical material that causes an intensity-dependent phase modulation. LC materials have a specific light intensity threshold that causes a phase transition in the molecules [33]. When the intensity is above this threshold value (high-intensity light), the molecules will undergo photoisomerization, which changes the refractive index of the local LC molecules. When the intensity is below the threshold value (low-intensity light), no photoisomerization occurs in the

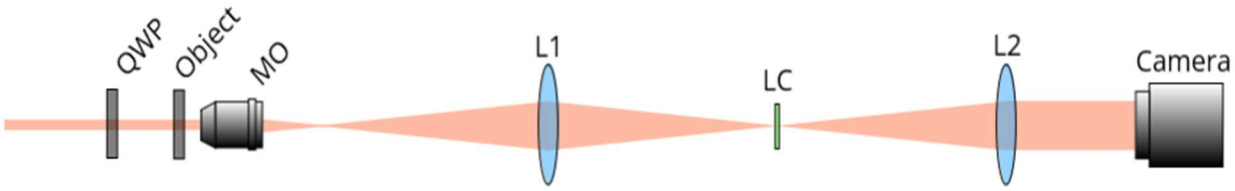

Figure 6
The laser is first sent through a QWP to circularly polarize the beam. The object is illumined by the beam and magnified by MO and L1. A liquid crystal is placed at the Fourier plane of L1 to phase shift the undiffracted light. The beam is then collimated by L2 and measured by a camera.

local LC molecules. This intensity-dependent property of the LC can be exploited to produce phase contrast images [34], [35]. By placing the LC at the Fourier plane, only undiffracted light will be above the intensity threshold and will be phase modulated [33].

An additional parameter exploited in this experiment is the optical anisotropy of the azobenzene liquid crystal material. For this purpose, the laser is first circularly polarized using the QWP. The object of interest (OI) is illuminated by the laser, and its image is magnified by a 20x objective and L1. Then the LC is placed at the Fourier plane of the image to phase shift the undiffracted light. This optical anisotropy of the liquid crystal will modulate all components of the circularly polarized light resulting in phase contrast images. Subsequently, L2 collimates the beam and the polarized camera captures four images at four linear stages of polarization (0°, 45°, 90°, and 135°). This results in four polarized images with different contrast that depends on the optical anisotropy and liquid crystal alignment.

We can then use the basics of interferometry and use the polarized images to calculate the phase map of the object using the following equation,

$$\Phi(\mathrm{x},\mathrm{y}) = \arctan\left(\frac{\mathrm{I(x,y,135°)-I(x,y,45°)}}{\mathrm{I(x,y,0°)-I(x,y,90°)}}\right), \tag{9}$$

where Φ is the wrapped phase map, and $I(x, y, \#°)$ are the camera images for each angle of polarization [14]. Equation 9 yields a phase map that is wrapped by 2π and is unwrapped using the unwrapping algorithm described in [36]. The process of taking an image and unwrapping it can be done relatively quickly to provide nearly real-time 3D information of an OI. Using the FLIR BFS-U3-51S5P-C camera with a resolution of 2448×2048, a frame rate of up to 4 fps was achieved.

Once a phase map is obtained and unwrapped, the thickness of the OI can be estimated. The accuracy of the system is determined by using phase maps to estimate the thickness of known

objects from a quantitative phase target [37]. Height estimates are made by first finding the mean phase value for the background of the image. Then the mean phase value for the OI is found. The absolute difference between the phase value for the OI and the background can be used, along with the wavelength of light and the refractive index, to estimate the thickness using the following relation,

$$\Delta\phi = \frac{\lambda}{2\pi}\Delta \mathrm{nd}, \tag{10}$$

where $\Delta\phi$ is the difference between the OI phase value and the background phase value, λ is the wavelength of light, Δn is the difference in refractive index between the OI and air, and d is the thickness of the OI [37].

First, a calibration is done on the system to determine its accuracy. A known quantitative phase benchmark [37] is used as the OI. The benchmark contains multiple types of target shapes of varying thicknesses. In this experiment, the 350 nm thick, group 6 element 2 of the 1951 USAF resolution test chart is used as the calibration target. The process described above will be used to calculate the quantitative phase information and estimate the thickness. The 350 nm target is used because it provides the largest signal-to-noise ratio in the phase measurement. The target is placed in the apparatus, and the phase information is reconstructed. Then, by comparing the expected phase difference to the experimentally measured phase difference, we can calculate a correction term to remove the systematic error. The correction term is calculated as follows,

$$\gamma = \frac{d_{exp}}{d_m}, \tag{11}$$

where γ is the correction term, d_{exp} is the expected thickness, and d_m is the measured thickness. After calibration, phase measurements of all the quantitative phase USAF targets, excluding the

350 nm calibration target, were taken to determine the accuracy of the system after calibration. The thicknesses are estimated using Equations 10 and 11 as follows,

$$d = \Delta\phi \frac{2\pi}{\lambda \Delta n} \gamma, \tag{12}$$

Once the calibration is completed, quantitative phase information is taken for HeLa cells. This measurement shows the aparatus' ability to gather quantitative phase information about a nearly transparent biological specimen. Then measurements of the thickness of an isopropyl alcohol droplet are taken during evaporation to demonstrate the apparatus' ability to measure quantitative phase information of a dynamic system. Isopropyl alcohol is atomized using a spray bottle and placed on a microscope slide. The alcohol droplets then evaporate over time due to the ambient air temperature.

CHAPTER 4: RESULTS AND DISCUSSION

Figure 7 shows the estimated thicknesses of the benchmark targets before and after calibration. There is a systematic error that causes the estimated thicknesses of each target to be off by about the same magnitude. The 350 nm object was measured to have a thickness of 764nm. Using Equation 11, the correction term γ is calculated to be 0.4581. The seven targets have the following thicknesses: 50 nm, 100 nm, 150 nm, 200 nm, 250 nm, 300 nm, and 350 nm. The estimated thicknesses are (42±22) nm, (85±34) nm, (151±61) nm, (216±54) nm, (243±68) nm, (318±34) nm, and (350±29) nm, respectively. The system estimated the thicknesses within 18nm across all targets. The mean value of double the standard deviation of the measurements is 86nm. 86nm is comparable with, or better than, all but two of the systems listed in Table 1, Phasefocus Livecyte and Phasics QPI. The 350 nm target was used to calibrate the system; therefore, the estimated thickness for that target is the same as expected.

Figure 8 shows the phase-contrast images for the 350 nm quantitative phase benchmark. There is an image for the four angles of polarization, 0°, 45°, 90°, and 135° as needed for the 4-step model. The phase information is then retrieved using Equation 9. The phase information for the 350 nm benchmark is shown in Figure 9. The width of each bar is approximately 7 μm. The measurement for the change in phase due to the object is (3.9440±0.3284) radians, therefore, using Equation 12, the estimated thickness is (350±29) nm. Figure 10 shows the phase information as a 3D surface with contour lines for every 50 nm thickness.

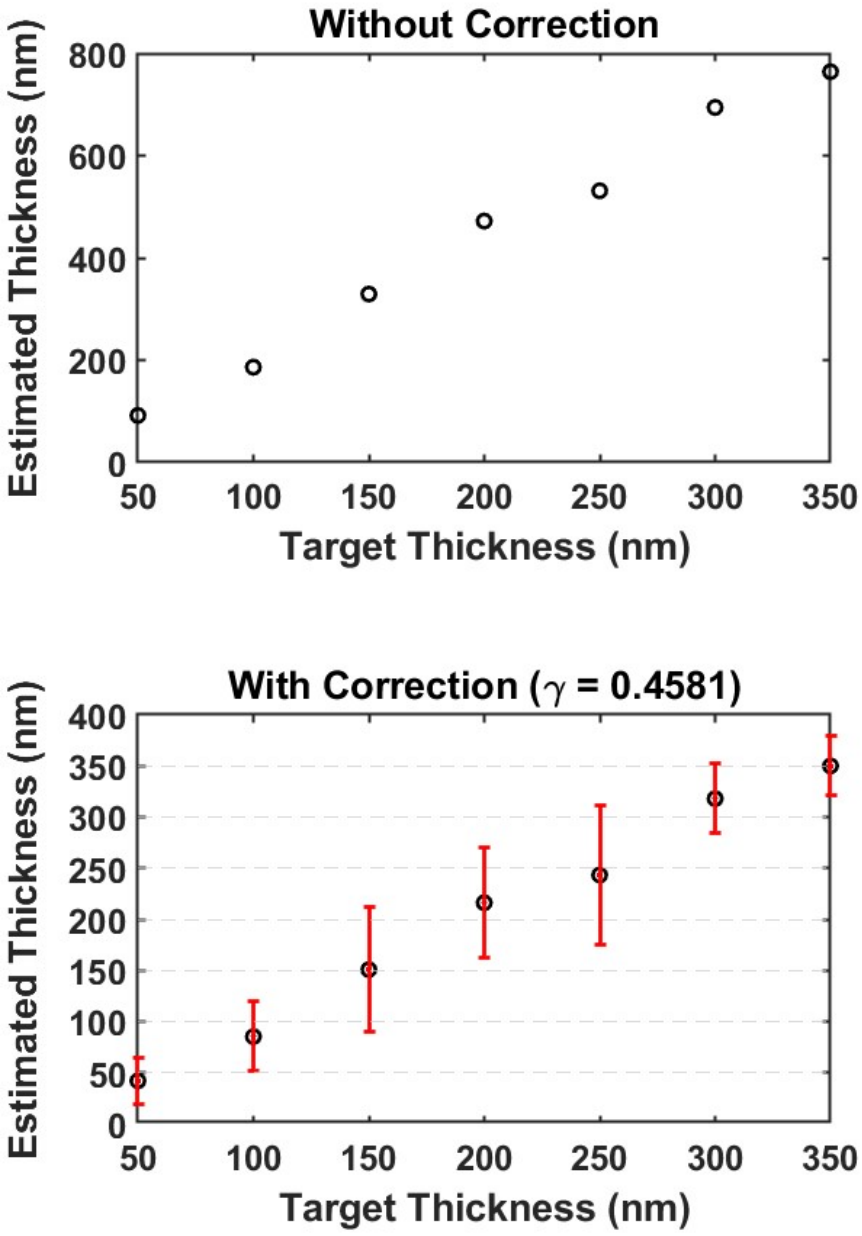

Figure 7
Measurements of the seven targets on the quantitative phase benchmark [37]. The seven targets have the following thicknesses: 50 nm, 100 nm, 150 nm, 200 nm, 250 nm, 300 nm, and 350 nm. The estimated thicknesses are (42±22) nm, (85±34) nm, (151±61) nm, (216±54) nm, (243±68) nm, (318±34) nm, and (350±29) nm, respectively. The 350 nm target is used in the calibration to find the correction term, γ, because it has the largest signal-to-noise ratio for the phase measurement.

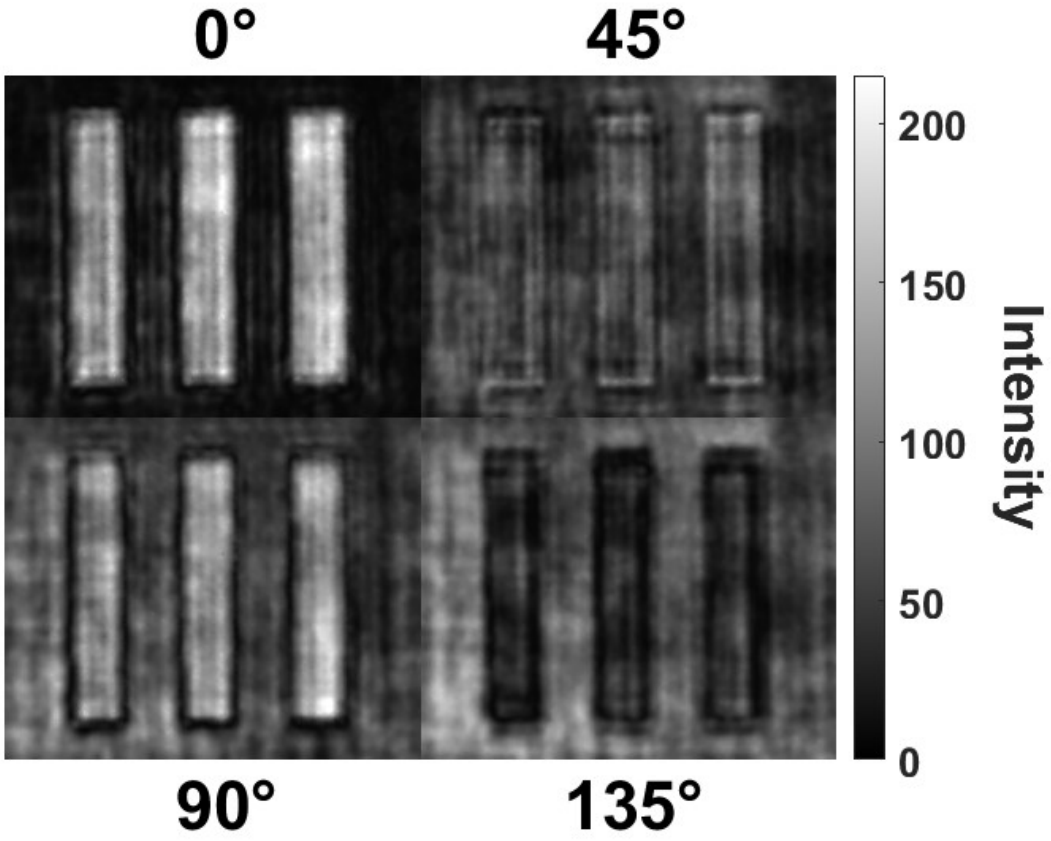

Figure 8
Phase-contrast images of group 6 element 2 from the 1951 USAF resolution test chart for a 350 nm quantitative phase target. The images were taken using a polarized camera that takes images at 4 angles of polarization: 0°, 45°, 90°, and 135°.

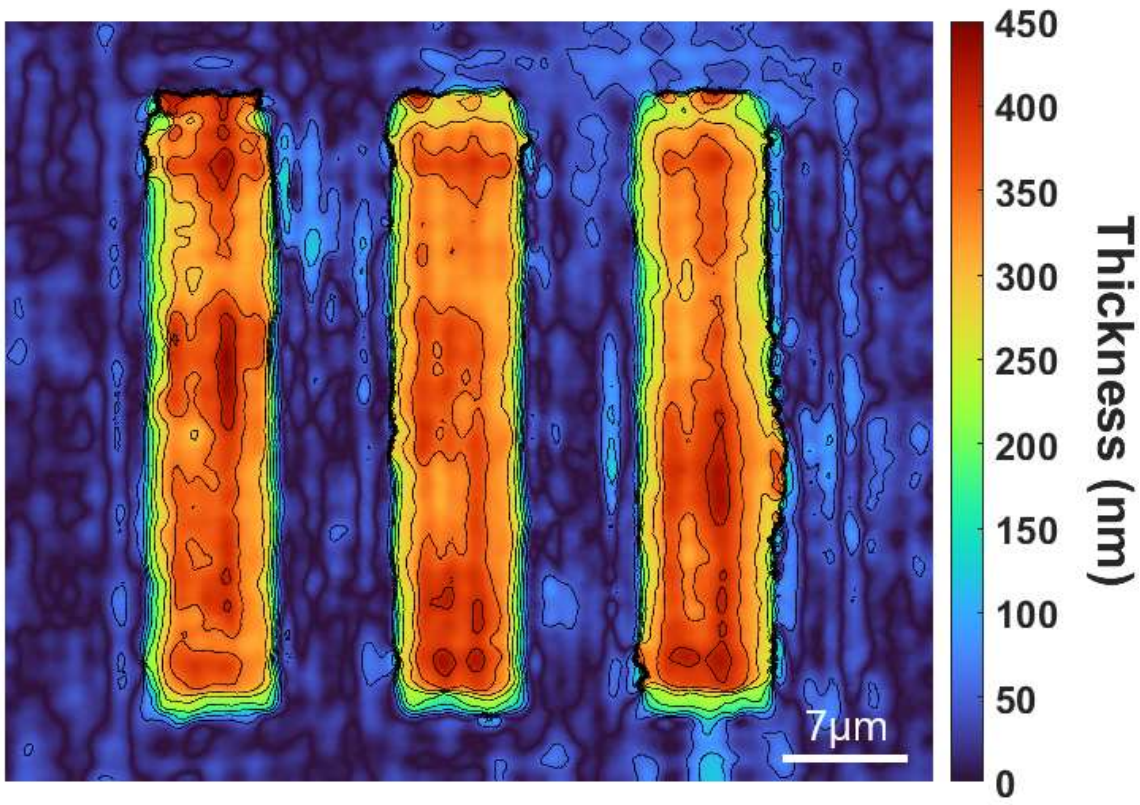

Figure 9
The unwrapped phase map for the 350 nm quantitative phase benchmark. The width of one bar is approximately 7 μm. The measurement for the object before calibration is (764±64) nm and (350±29) nm after calibration.

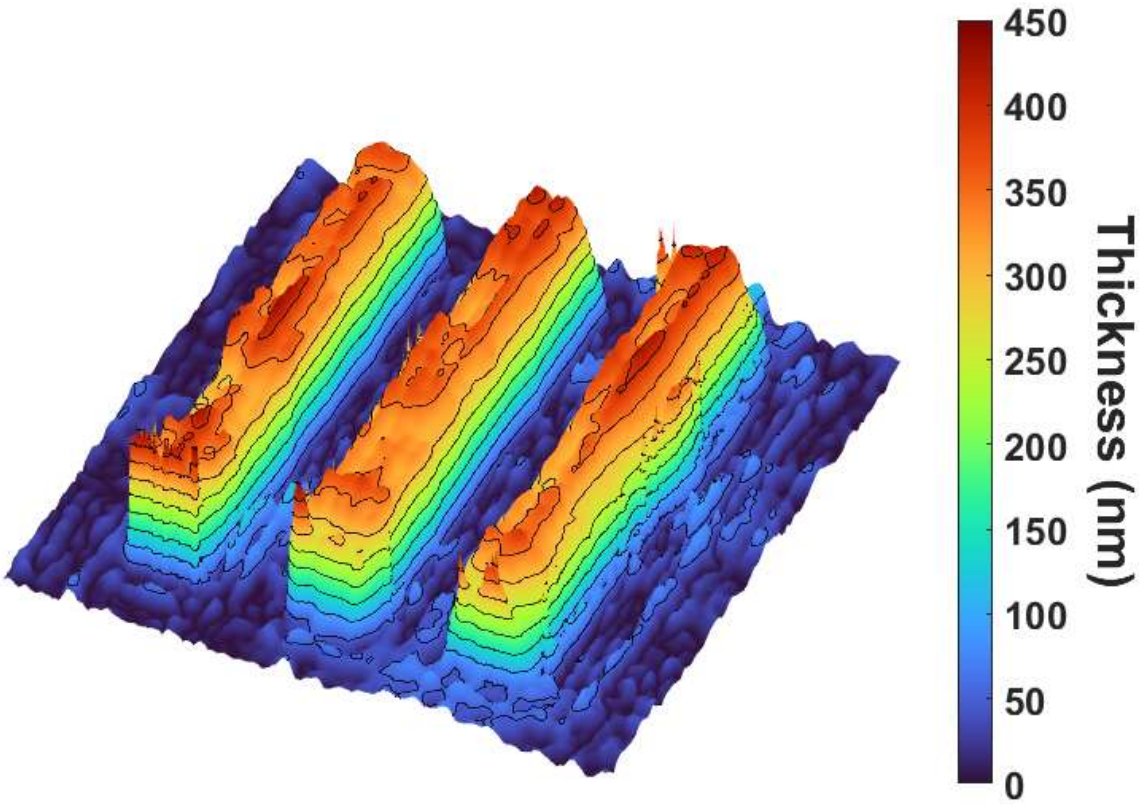

Figure 10
The unwrapped phase map for the 350 nm quantitative phase benchmark is shown as a 3D surface. The width of one bar is approximately 7 μm. The spacing between contour lines is 50 nm. The measurement for the object before calibration is (764±64) nm and (350±29) nm after calibration.

Figure 11 shows the phase-contrast images of the HeLa cells. There is an image for the four angles of polarization, 0°, 45°, 90°, and 135°. Using Equation 9, these phase-contrast images can be used to calculate the phase information of the HeLa cells, as shown in Figure 12 and Figure 13. A couple of the cells at the bottom of Figure 12 induced a phase shift of approximately 2.8π at the center of the cell where the nucleus is located. The other cells induced a maximum phase shift of approximately 1.2π to 2π around their nucleus.

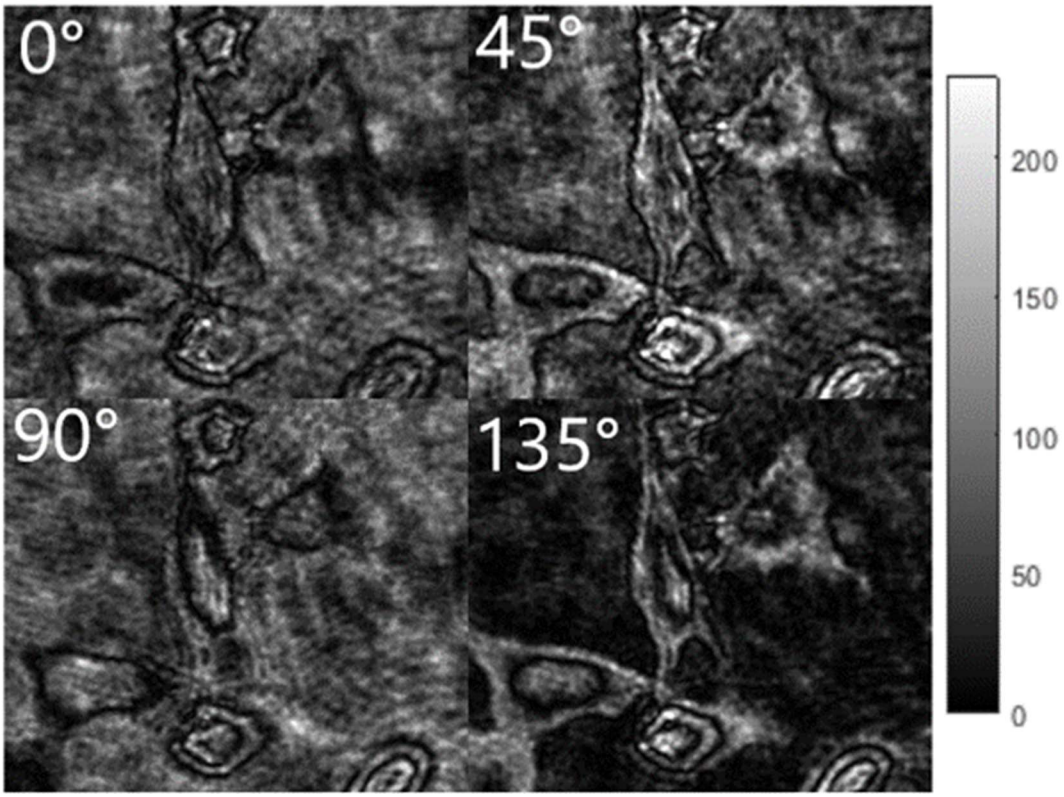

Figure 11
Phase-contrast images of HeLa cells. The images were taken using a polarized camera that takes images at 4 angles of polarization: 0°, 45°, 90°, and 135°.

The 3D phase information of an evaporating isopropyl alcohol droplet is shown in Figure 13. The thickness of the droplet at t = 0 s is approximately 425 nm, and over 40 s the droplet evaporates. At t = 20 s the droplets shrink to a thickness of approximately 300 nm. By t = 40 s the droplet has completely evaporated. Figure 15 shows more detailed information about the thickness of the alcohol droplet before, during, and after the evaporation. The images in Figure 14 were taken during times t = 60 s, 80 s, and 100 s from the data in Figure 15. Figure 15 shows that the alcohol drop was sitting consistently around 425 nm before the evaporation started at t = 60 s. By

t = 100 s the droplet had completely evaporated and the estimated thickness was around 60 nm which is within the noise range of the background phase.

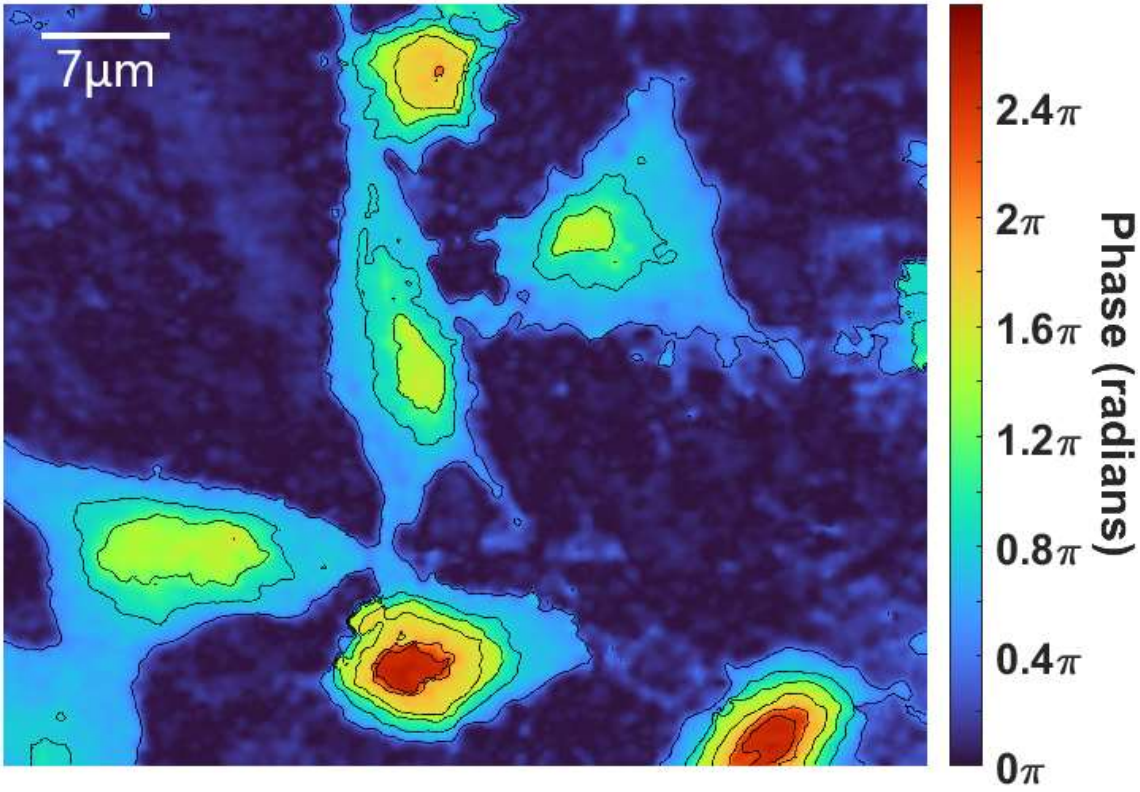

Figure 12
The unwrapped phase map for an image of several HeLa cells is shown. The maximum phase change caused by the cells is ~2.8π. Some of the smaller cells caused approximately 1.2π to 2π of phase modulation.

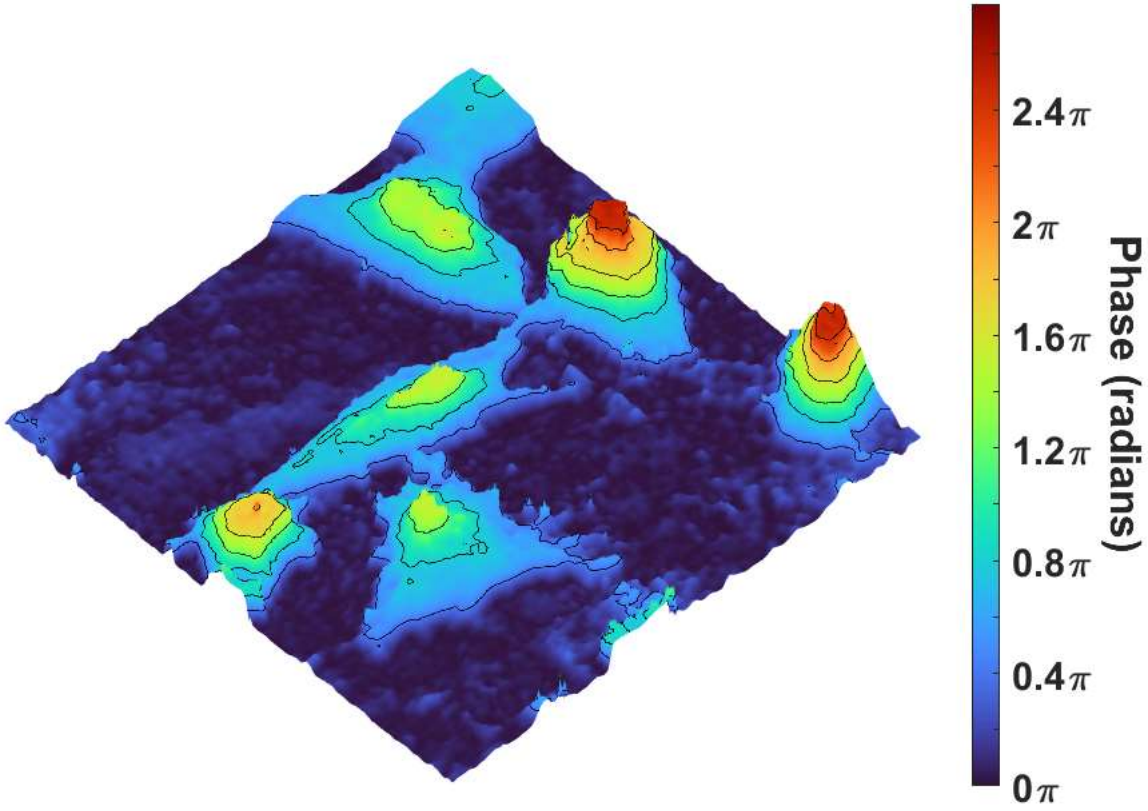

Figure 13
A 3D surface plot of the HeLa cells is shown. The maximum phase change caused by the cells is ~2.8π. Some of the smaller cells caused approximately 1.2π to 2π of phase modulation.

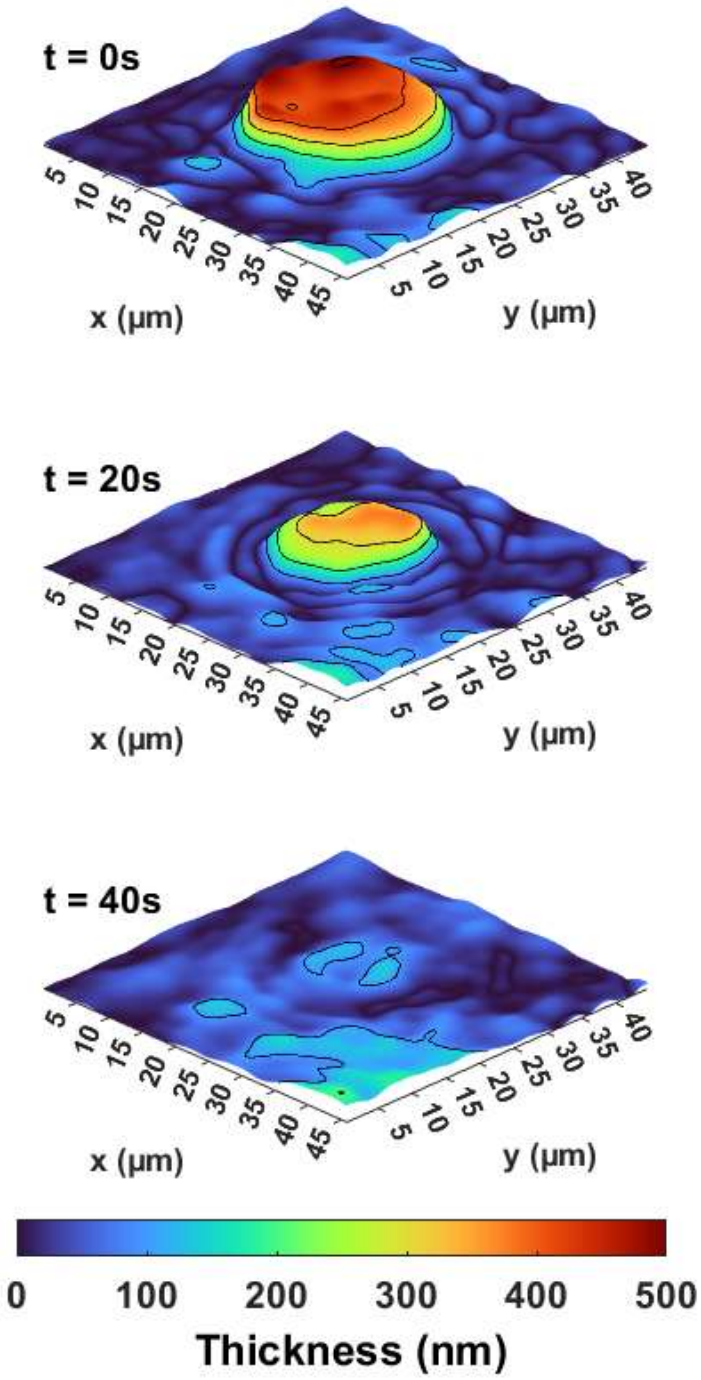

Figure 14
An isopropyl alcohol drop is shown to evaporate over time. At t = 0 s, the drop has a thickness of ~425 nm. At t = 20 s, the drop has a thickness of ~300 nm. At t = 40 s, the drop is completely evaporated.

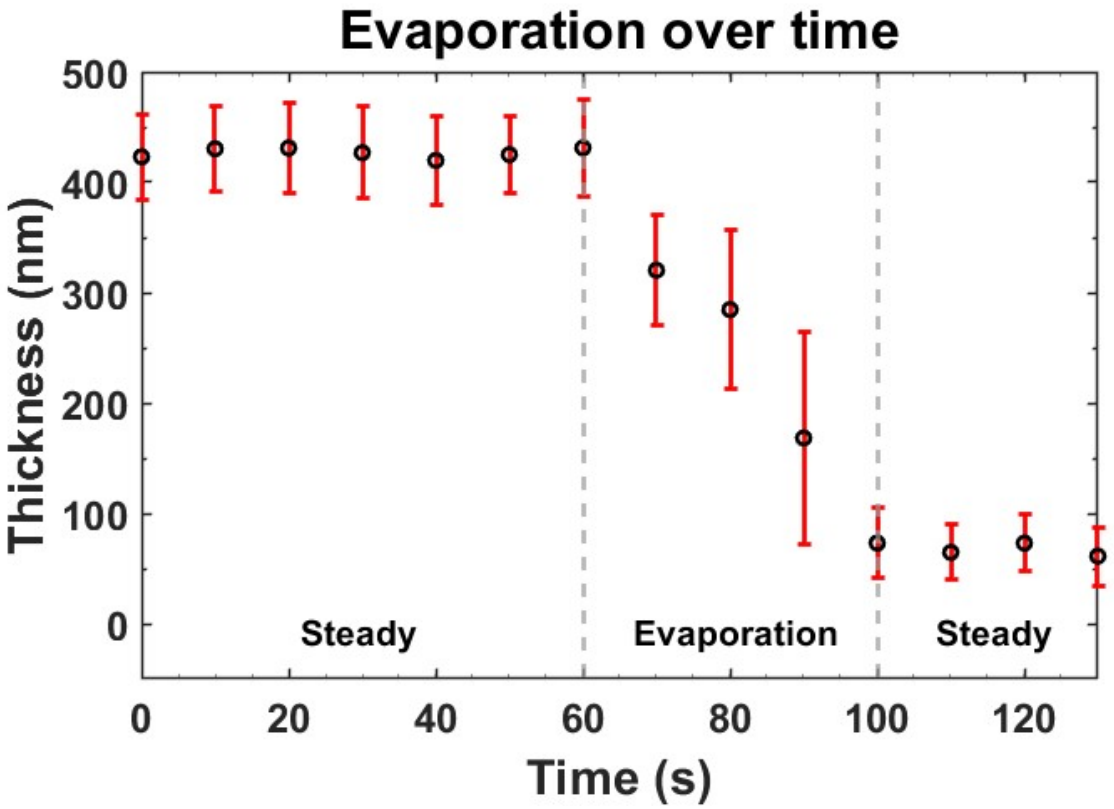

Figure 15
An isopropyl alcohol droplet is shown to evaporate over time. The thickness of the alcohol droplet is approximately 425 nm. At t = 60 s, the alcohol droplet begins evaporating. The alcohol droplet evaporates and loses thickness between t = 60 s and t = 100 s. Evaporation stops at t = 100 s.

CHAPTER 5: CONCLUSIONS

This work provides the proof-of-principle of QPM using azobenzene liquid crystals in a single shot enabling dynamic phase measurements of transparent objects. This system has demonstrated its ability to accurately and dynamically measure phase information from POs. Measurements of the quantitative phase benchmark show that this system can provide thickness estimations within 10's of nanometers of the expected value. The measurements of the HeLa cells indicate that the system can obtain detailed phase information from a complex PO. Measurements of the evaporating alcohol droplet show the system's ability to measure quantitative phase information quickly from a dynamic object due to the ability to get the phase-contrast images in a single-shot. This system is inexpensive compared to the commercially available QPI systems shown as the entire system costs less than $10,000. The technique is also comparable to, or better than, the accuracy of the commercial systems. Lastly, the techniques used are non-invasive, compact, and robust to environmental noise due to the CPC.

The phase reconstruction can be further improved by increasing the contrast in the phase-contrast images. This improvement can come from exploring different LC materials. LCs with optical properties might be more suitable for generating contrast in this context. Certain LCs might also provide more homogeneity and less background noise, which would improve image contrast.

Another possible improvement can be made by obtaining more phase-contrast images before calculating the phase. The more images that are obtained, the more accurate the calculated phase maps will be. One way this can be implemented is to use a beam splitter to send one beam to a camera and another beam to a camera at 22.5° rotation relative to a second polarized camera. This would yield eight images with a $\pi/4$ shift relative to one another. Again, using a model that can take advantage of the additional images will make the resulting phase maps more accurate.

REFERENCES

[1] D. O. Lapotko and V. P. Zharov, "Spectral evaluation of laser-induced cell damage with photothermal microscopy," *Lasers Surg Med*, vol. 36, no. 1, pp. 22–30, Jan. 2005, doi: 10.1002/lsm.20119.

[2] M. Mir, B. Bhaduri, R. Wang, and R. Zhu, *Quantitative Phase Imaging*, vol. 57. Elsevier Inc., 2012. doi: 10.1016/B978-0-44-459422-8.00003-5.

[3] Z. Wang *et al.*, "Spatial light interference microscopy (SLIM)," 2011.

[4] C. Seniya, C. E. Towers, and D. P. Towers, "Low cost label-free live cell imaging for biological samples," in *Quantitative Phase Imaging III*, SPIE, Feb. 2017, p. 100741I. doi: 10.1117/12.2246680.

[5] R. Porras-Aguilar *et al.*, "Polarization-controlled contrasted images using dye-doped nematic liquid crystals," *Opt Express*, vol. 17, no. 5, p. 3417, 2009, doi: 10.1364/oe.17.003417.

[6] F. Zernike, "How I Discovered Phase Contrast," *Science (1979)*, vol. 121, no. 3141, pp. 345–349, Mar. 1955.

[7] K. Lee *et al.*, "Quantitative Phase Imaging Techniques for the Study of Cell Pathophysiology: From Principles to Applications," *Sensors*, vol. 13, no. 4, pp. 4170–4191, 2013, doi: 10.3390/s130404170.

[8] B. Bhaduri *et al.*, "Diffraction phase microscopy: principles and applications in materials and life sciences", doi: 10.1364/AOP.6.000057.

[9] N. T. Shaked, I. Barnea, and N. T. Shaked, "Label-Free Quantitative Imaging of Sperm for In-Vitro Fertilization Using Interferometric Phase MicroscopyIVF, IMSI, ICSI, IPM, Holography, Imaging, Sperm," *Journal of Fertilization: In Vitro - IVF-Worldwide, Reproductive Medicine, Genetics & Stem Cell Biology*, vol. 4, no. 3, pp. 1–6, Aug. 2016, doi: 10.4172/2375-4508.1000190.

[10] G. Popescu, T. Ikeda, R. R. Dasari, and M. S. Feld, "Diffraction phase microscopy for quantifying cell structure and dynamics," *Opt Lett*, 2006, doi: 10.1364/OL.31.000775.

[11] G. Popescu, *Quantitative phase imaging of cells and tissues*. McGraw-Hill, 2011.

[12] E. Mavrona *et al.*, "Intrinsic and photo-induced properties of high refractive index azobenzene based thin films [Invited]," *Opt Mater Express*, vol. 8, no. 2, p. 420, 2018, doi: 10.1364/ome.8.000420.

[13] A. Galeana and R. Porras-Aguilar, "Real-time label-free microscopy with adjustable phase-contrast," *Opt Express*, vol. 28, no. 19, p. 27524, 2020, doi: 10.1364/oe.398748.

[14] K. Creath, "V Phase-Measurement Interferometry Techniques," *Progress in Optics*, vol. 26, no. C, pp. 349–393, 1988, doi: 10.1016/S0079-6638(08)70178-1.

[15] "Livecyte." https://www.phasefocus.com/livecyte

[16] "Tomocube." https://www.tomocube.com/product/ht-series/#HT_series_cont

[17] "Lyncée Tec." https://www.lynceetec.com/reflection-dhm/#tab-2

[18] "Holomic." https://holomic.com/content/home

[19] "Phase Holographic Imaging PHI AB." https://phiab.com/holomonitor/

[20] "Phasics." https://www.phasics.com/en/application-areas/quantitative-phase-imaging/

[21] J. Glückstad and P. C. Mogensen, "Optimal phase contrast in common-path interferometry," 2001.

[22] A. Galeana and R. Porras-Aguilar, “Real-time label-free microscopy with adjustable phase-contrast,” *Opt Express*, vol. 28, no. 19, p. 27524, Sep. 2020, doi: 10.1364/oe.398748.
[23] R. Porras-Aguilar, K. Falaggis, J. C. Ramirez-San-Juan, and R. Ramos-Garcia, “Self-calibrating common-path interferometry,” *Opt Express*, vol. 23, no. 3, p. 3327, Feb. 2015, doi: 10.1364/oe.23.003327.
[24] R. G. Porras-Aguilar, “LIQUID CRYSTAL REORIENTATION INDUCED BY PHOTOISOMERIZATION AND ITS APPLICATIONS IN IMAGE PROCESSING,” Instituto Nacional de Astrofísica, Óptica y Electrónica, Puebla, 2009.
[25] I. C. Khoo, *Liquid Crystals: Physical properties and nonlinear optical phenomena*, 4th ed., . 4th ed., John Wiley & Sons, 1995.
[26] Uladzimir A. Hrozhyk, Svetlana V. Serak, Nelson V. Tabiryan, Landa Hoke, Diane M. Steeves, and Brian R. Kimball, “Azobenzene liquid crystalline materials for efficient optical switching with pulsed and/or continuous wave laser beams,” *Opt Express*, vol. 18, no. 8, pp. 8697–8704, 2010.
[27] G. H. Brown, *Techniques of Chemistry, Vol. III, Photochromism*. New York: John Wiley & Sons, 1971.
[28] L. Komitov, K. Ichimura, and A. Strigazzi, “Light-induced anchoring transition in a 4,4’-disubstituted azobenzene nematic liquid crystal,” *Liq Cryst*, vol. 27, no. 1, pp. 51–55, 2000, doi: 10.1080/026782900203209.
[29] L. Komitov, C. Ruslim, Y. Matsuzawa, and K. Ichimura, “Photoinduced anchoring transitions in a nematic doped with azo dyes,” *Liq Cryst*, vol. 27, no. 8, pp. 1011–1016, 2000, doi: 10.1080/02678290050080733.
[30] S. V Serak, N. V Tabiryan, T. J. White, and T. J. Bunning, “Azobenzene liquid crystal polymer-based membrane and cantilever optical systems,” 2009.
[31] Gabriel Popescu, *Quantitative Phase Imaging of Cells and Tissues*, 1st ed., . 1st ed., New York City: McGraw-Hill, 2011.
[32] Y. Park *et al.*, “Diffraction phase and fluorescence microscopy References and links,” 2006.
[33] C. S. Yelleswarapu, S. R. Kothapalli, F. J. Aranda, D. V. G. L. N. Rao, Y. R. Vaillancourt, and B. R. Kimball, “Phase contrast imaging using photothermally induced phase transitions in liquid crystals,” *Appl Phys Lett*, vol. 89, no. 21, 2006, doi: 10.1063/1.2397030.
[34] L. A. DeMars, M. Mikuła-Zdańkowska, K. Falaggis, and R. Porras-Aguilar, “Single-shot phase calibration of a spatial light modulator using geometric phase interferometry,” *Appl Opt*, vol. 59, no. 13, p. D125, 2020, doi: 10.1364/ao.383610.
[35] L. A. Alemán-Castaneda, B. Piccirillo, E. Santamato, L. Marrucci, and M. A. Alonso, “Shearing interferometry via geometric phase,” *Optica*, vol. 6, no. 4, p. 396, 2019, doi: 10.1364/optica.6.000396.
[36] J. Martinez-Carranza, K. Falaggis, and T. Kozacki, “Fast and accurate phase-unwrapping algorithm based on the transport of intensity equation,” *Appl Opt*, vol. 56, no. 25, p. 7079, 2017, doi: 10.1364/ao.56.007079.
[37] Z. F. Phillips and M. Chen, “Technical Report : Benchmark Technologies Quantitative Phase Target,” 2017.